The High W Challenge: Robust Neutrino Energy Estimators for LArTPCs

Christopher Thorpe[1], Elena Gramellini[1]

[1]*The University of Manchester, Manchester M13 9PL, UK*

(Dated: November 17, 2025)

Accurate determination of the neutrino energy is central to precision oscillation measurements. In this work, we introduce the W^2-based estimator, a new neutrino energy estimator based on the measurement of the final-state hadronic invariant mass. This estimator is particularly designed to be employed in liquid-argon time-projection chambers exposed to broadband beams that span the challenging transition region between shallow inelastic scattering and deep inelastic scattering. The performance of the W^2-based estimator is compared against four other commonly used estimators. The impact of the estimator choice is evaluated by performing measurements of δ_{CP} and Δm_{23}^2 in a toy long-baseline oscillation analysis. We find that the W^2-based estimator shows the smallest bias as a funciton of true neutrino energy and it is particularly stable against the mismodelling of lepton scattering angle, missing energy, hadronic invariant mass and final state interactions. Such an inclusive channel complements well the strength of more exclusive methods that optimizes the energy resolution. By providing a detailed analysis of strengths, weaknesses and domain of applicability of each estimator, this work informs the combined used of energy estimators in any future LArTPC-based oscillation analysis.

I. INTRODUCTION

Neutrino oscillations are the only evidence of beyond the Standard Model (BSM) reproducible in the laboratory and provide a unique window into unresolved questions in neutrino physics, such as the ordering of neutrino masses and the potential for CP violation in the lepton sector [1].

In a simplified but pedagogically useful scenario, the oscillations probability between two neutrinos of different flavors can be expressed as:

$$P(\nu_\alpha \to \nu_\beta) = \sin^2(2\theta)\sin^2\left(1.27\frac{\Delta m_{21}^2\ L\,[\mathrm{km}]}{E_{\mathrm{true}}\,[\mathrm{GeV}]}\right), \quad (1)$$

where L is the baseline (source-to-detector distance), E_{true} is the **true** neutrino energy, θ is the mixing angle, and Δm_{21}^2 is the squared mass difference between the two neutrino mass eigenstates. While the oscillation probability is a function of the true neutrino energy, E_{true}, detectors can only measure visible final state quantities to estimate the neutrino energy, E_{est}. The relationship between these quantities is nontrivial, reflecting the combined effects of the incident neutrino flux and of neutrino–nucleus interactions even before accounting for detector response.

Current and future accelerator-based neutrino experiments such as the Short-Baseline Neutrino (SBN) [2] program and the Deep Underground Neutrino Experiment (DUNE) [3, 4] benefit from the use of broadband energy beams, which enable the sampling of multiple oscillation maxima. This approach enhances sensitivity to oscillation parameters, including CP-violating phases and the neutrino mass ordering. Its drawback, however, is that a wide neutrino energy spectrum inevitably samples a broad range of neutrino–nucleus interaction channels. These span from charged-current quasi-elastic (CCQE) scattering at lower energies, through baryonic resonance production (RES) and meson-exchange current (MEC) processes, up to deep inelastic scattering (DIS) at higher energies. The overlapping nature of these regimes complicates both the modeling of interaction dynamics and the reconstruction of the incident neutrino energy, which is essential for precise oscillation analyses. While previous work has focused on exclusive channels [5] or on advanced machine learning reconstruction techniques [6], we are interested in exploring more inclusive channels, which, by definition, improve of the sample statistics. We assume that ongoing progress in LArTPC reconstruction algorithms will eventually enable high-fidelity reconstruction of most events. Under these conditions, more inclusive analyses may prove to be not only statistically advantageous but also resilient to model and detector-related uncertainties.

This paper explores a new approach to analyzing the final state kinematics, based on the calculation of the final state hadronic invariant mass. This method targets high hadron multiplicity events expected from the interactions of multi-GeV neutrinos in future LArTPCs. This method is then benchmarked against several established methods of estimating neutrino energy, introduced in Section III. Since we lack direct access to nature's true interaction dynamics, we rely on several event generators, each of which embodies different theoretical assumptions to probe different kinematic scenarios as a function of the true energy. The different event generators employed in this study are introduced in Section II, together with the adopted reconstruction assumptions. We compare the performance of the different estimators by first calculating their bias and variance with respect to neutrino energy in Section V, and then with respect to other kinematic variables in Section VI. Finally, we assess their impact on oscillation measurements through a series of tests presented in Sections VII and VIII.

II. SIMULATION OF NEUTRINO EVENTS

The evaluation of neutrino energy estimators necessarily relies on a set of working assumptions. As a case study, we adopt the neutrino flux provided by the DUNE Collaboration [3], without including the effects of oscillation outside of the studies presented in Sections VII and VIII. We restrict the true neutrino energies to the range 0.5–6 GeV, which is most relevant for oscillation measurements. Any comparable flux that covers the shallow to deep inelastic transition region would serve equally well for the purposes of this study. The neutrino–nucleus interaction models are listed in Section II A, and our idealized particle reconstruction is outlined in Section II B. These ingredients provide a controlled environment in which to test and compare the five different estimators of the neutrino energy.

A. Event generators

Simulations were conducted with four neutrino interaction event generators:

- GENIE version 3.6.2 [7], from which we use the `G18_10a_02_11a` tune.

- NuWro 25.03.1 [8].

- NEUT version 5.8.0 [9].

- GiBUU 2025 [10].

We use the default settings for NuWro, NEUT and GiBUU. These generators provide varied interaction models and event topologies, allowing a thorough estimator performance analysis.

B. Reconstruction Assumptions

In this work, we assume an idealized particle reconstruction accuracy, in which the detection of final-state particles is taken to be 100% efficient above the set of realistic detector thresholds reported in Table I. The adopted thresholds are consistent with literature [11] and motivated by expected capabilities for future LArTPCs [3]. In all calculations, we neglect rare final state particles such as kaons and hyperons and we assume neutrons are not detected.

TABLE I. Detection thresholds for perfect reconstruction, with values corresponding to the momentum energy of each particle.

	p	$\pi^\pm$	π^0	μ	e
Thresholds (GeV)	0.3	0.1	0.0	0.1	0.05

Although these assumptions do not represent the true performance of any detector, they provide a useful starting point for understanding the energy reconstruction techniques under study.

Unless otherwise stated, we assume perfect kinematic reconstruction of particles above the thresholds in Table I. When discussing the impact of detector resolution effects on neutrino energy estimation, we assume the momentum resolutions shown in Table. II. These are estimated from the performance of the MicroBooNE detector on fully contained particles [12–15]. Additionally, when considering the calorimetric method introduced in Section III D, we assume a resolution on the total energy of 20%. This choice is justified by the recent MicroBooNE results in Ref. [15, 16].

TABLE II. Momentum resolutions for the measurements of different final state particles used to estimate neutrino energy. When applying the total visible energy method, we also assume an overall energy resolution of 20%.

	p	$\pi^\pm$	π^0	μ	e
Resolution (%)	15	25	25	10	10

III. ENERGY ESTIMATORS

We compare five energy estimators: (i) one that assumes all interactions are CCQE-like (*CCQE-like estimator*); (ii) a new approach that improves on the CCQE-like estimator by accounting for multiproton knockout and pion-producing interactions through the hadronic invariant mass (W^2 *estimator*); (iii) the sum of the lepton energy and proton kinetic energies (*proton-based estimator*); (iv) the total energy of all final-state particles, intended to mimic calorimetric reconstruction (*calorimetric method*); and (v) the Sobczyk–Furmanski method [5] (*SF Estimator*).

A. CCQE-like Estimator

This estimator assumes charged-current quasi-elastic (CCQE) kinematics to reconstruct neutrino energies, predominantly using the lepton momentum and deflection angle with respect to the beam direction. The estimated neutrino energy ($E_{\text{est}}^{\text{CCQE}}$) is defined as:

$$E_{\text{est}}^{\text{CCQE}} = \frac{m_p^2 - (m_n - E_b)^2 - m_l^2 + 2(m_n - E_b)E_l}{2(m_n - E_b - E_l + p_l \cos\theta_l)},$$
(2)

where m_p, m_n, and m_l are the masses of the proton, neutron, and scattered charged lepton, respectively, E_b is a binding energy correction which we take to be 30 MeV for argon, and E_l, p_l, and θ_l are the energy, momentum, and scattering angle of the charged lepton.

B. W^2-based Estimator

The W^2-based estimator improves on the CCQE-like method through utilization of the visible hadronic invariant mass(W_{vis}) to expand the methods assumptions and include meson producing interactions. The initial state mass is adjusted according to the number of visible final state protons to account for the existence of multi-nucleon knockout interactions. The expression for the estimated energy $\left(E_{\mathrm{est}}^{W^2}\right)$ is:

$$E_{\mathrm{est}}^{W^2} = \frac{W_{\mathrm{vis}}^2 - n_p^2(m_n - E_b)^2 - m_l^2 + 2n_p(m_n - E_b)E_l}{2(n_p m_n - n_p E_b - E_l + p_l \cos\theta)},$$

(3)

where n_p is the number of visible protons in the final state and W_{vis} is the visible hadronic invariant mass. This method is only applied to final states with at least one visible proton.

C. Proton-Based Estimator

Designed specifically for low-energy neutrino interactions, this estimator combines detailed track reconstruction with calorimetric measurements. The expression for the estimated energy ($E_{\mathrm{est}}^{\mathrm{PB}}$) in this instance is given by the lepton total energy (E_l) plus the sum of the kinetic energies of all visible protons (E_k):

$$E_{\mathrm{est}}^{\mathrm{PB}} = E_l + \sum_{\mathrm{protons}} E_k.$$

(4)

Similar to the method used in the MicroBooNE analyses testing the MiniBooNE anomaly [17, 18], this estimator is only be applied to the exclusive topologies containing no visible mesons in the final state.

D. Calorimetric Method

Experiments relying on the detection of exclusively DIS events, such as IceCube, typically employ calorimetry or quantities analogous to calorimetric information. This method is distinguished from the others in this review in that high level reconstructed objects such as individual particle kinematics are not required; the energy measurement can be performed in a LArTPC by measuring the total charge collected by the readout.

In this case, the neutrino energy is estimated by summing the measured muon and hadronic energy deposits. Thus, we model the behavior of this estimator by summing the total energy of the lepton, the kinetic energies of all visible protons, and the total energies of all visible pions. The expression for the estimated energy ($E_{\mathrm{est}}^{\mathrm{SKE}}$) is thus given by the lepton total energy (E_l) plus the sum of the kinetic energies of all visible protons (E_k) and pions (E_π):

$$E_{\mathrm{est}}^{\mathrm{SKE}} = E_l + \sum_{\mathrm{protons}} E_k + \sum_{\mathrm{pions}} E_\pi.$$

(5)

Unlike the other methods explored in this paper, this method does not rely on high level reconstructed objects such as particle tracks or electromagnetic showers.

E. Sobczyk-Furmanski Estimator

The Sobczyk-Furmanski (SF) method [5] analyses the energy balance by separating the kinematics into transverse (T) and longitudinal (L) components, to infer the additional energy supplied by the motion of the struck nucleon. The neutrino energy is expressed in terms of the mass of the parent nucleus, M_A, the mass of the daughter nucleus M_{A-1}, and the combined transverse/longitudinal momenta of the lepton-proton system, $p^{T,L} = p_{\mathrm{prot}}^{T,L} + p_l^{T,L}$. The estimated neutrino energy ($E_{\mathrm{est}}^{\mathrm{SF}}$) is then obtained from the following expressions:

$$p^L = \frac{(M_A + p_l^L + p_{\mathrm{prot}}^L - E_l - E_{\mathrm{prot}})^2 - (p^T)^2 - M_{A-1}^2}{2(M_A + p_l^L + p_{\mathrm{prot}}^L - E_l - E_{\mathrm{prot}})},$$

(6)

$$E_{\mathrm{est}}^{\mathrm{SF}} = p_l^L + p_{\mathrm{prot}}^L - p^L.$$

(7)

This estimator is only be applied to exclusive topologies containing a single visible proton and the charged lepton.

F. Inclusivity Considerations

An important factor in comparing different energy estimation techniques is the degree of inclusiveness of the event sample to which each method can be validly applied, as this directly impacts the available statistics. The CCQE-like and SKE estimators are valid for all hadronic final states, though the CCQE-like estimator is not expected for perform well on events that are not true CCQE. The W^2 and proton-based estimators both require at least one visible proton, with the latter additionally requiring the absence of visible pions. The SF estimator is the most exclusive, requiring a clean topology with exactly one visible proton and no pions.

While the total predicted cross section is relatively consistent across generators, there are substantial variations in the predicted exclusive channels. This is illustrated in Fig. 1, which shows the fractions of events producing final states with at least one proton and any number of pions (Np), at least one proton and no pions (Np0π), and exactly one proton and no pions (1p0π). This shows substantial loss of statistics in the multi-GeV region when excluding events with final state pions, where the second oscillation maximum is expected to appear at DUNE's baseline.
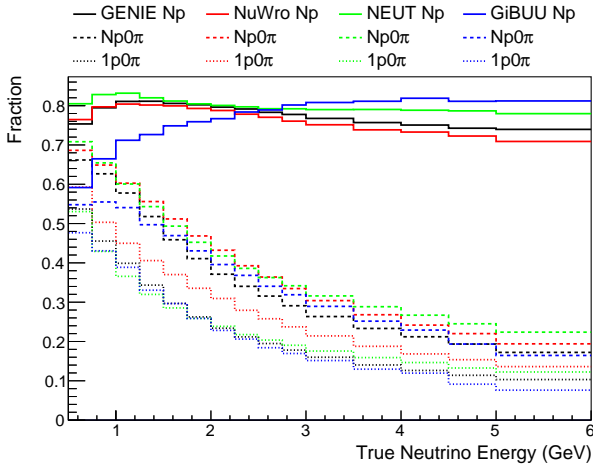
FIG. 1. Fractions of ν_μ interactions on argon that produce final states with at least one proton (Np), at least one proton and no pions (Np0π), and exactly one proton and no pions (1p0π). The latter two categories reflect the subsets of events the proton based and SF methods target.

IV. RESPONSE MATRICES

To understand the basic characteristics of each energy estimation method, we begin by calculating the corresponding response matrix. Defined as

$$R(E_\text{est}, E_\text{true}) = \text{Prob}(E_\text{est}|E_\text{true}), \quad (8)$$

the response matrix represents the probability that a neutrino of true energy E_true is reconstructed with an estimated energy E_est. These matrices are normalized such that $\int R(E_\text{est}, E_\text{true})dE_\text{est} = 1$ regardless of the selection criteria applied to the underlying samples; the total number of events in each matrix thus reflects the degree of inclusiveness required by the corresponding energy estimator. Fig. 2 shows the response matrices for the five energy estimators, using events simulated with GENIE. Response matrices calculated with the other three generators can be found in the Supplemental Material [19].

The matrix for the CCQE-like estimator exhibits a pronounced secondary band offset from the diagonal, primarily arising from multiproton knockout events and final states containing pions—processes neglected by this method. In contrast, the W^2 estimator, which is based on similar assumptions but explicitly accounts for pion production and multiproton events, shows a single, well-defined diagonal peak.

The proton-based, SF, and calorimetric estimators all feature narrow diagonal peaks and a significant population in the lower-right quadrant. This reflects that these methods essentially reconstruct the time component of the total final-state four-momentum, which equals the true neutrino energy in the absence of FSI, nucleon motion, or undetected particles. The off-diagonal population arises from events affected by FSI, which are challenging to model. The influence of FSI on the differ-

ent estimators is discussed further in Section V C. The proton-based and SF estimators also appear more effective at higher energies, as indicated by the narrowing of their distributions above approximately 4 GeV. However, this trend primarily reflects the diminishing number of events to which these estimators can be applied at such energies, implying that highly pure event selections will be required for their effective use in this regime.

The fractional error, defined as $(E_\text{est} - E_\text{true})/E_\text{true}$, further illustrates how the choice of estimator and the inclusion of resolution effects influence neutrino energy reconstruction. Figure 3 shows the fractional error distributions for the different estimators obtained using GENIE, assuming perfect kinematic resolutions in Fig. 3(a), and after applying smearing effects in Fig. 3(b). The results for other generators are provided in the Supplementary Material [19]. Assuming perfect kinematic reconstruction, the proton-based, SF, and calorimetric estimators exhibit the best performance. However, the calorimetric method is particularly sensitive to resolution effects associated with energy deposition in LArT-PCs, as evident from the comparison between Figs. 3(a) and 3(b). The CCQE-like estimator shows a narrow peak near zero with a pronounced asymmetric tail, corresponding to CCQE and non-CCQE interactions, respectively. A comparison between the CCQE-like and W^2 estimators highlights the improvement gained by incorporating the invariant mass into the energy reconstruction. Both produce similarly shaped peaks near zero, but the W^2 method notably lacks the long tail characteristic of the CCQE-like estimator.

V. BIAS, AND VARIANCE

We further compare the effectiveness of different neutrino energy estimators by calculating the fractional bias $B(E_\text{true})$ and fractional variance $V(E_\text{true})$ of each estimator as a function of true neutrino energy. These are defined as:

$$B(E_\text{true}) = \int R(E_\text{est}, E_\text{true}) \left(\frac{E_\text{est} - E_\text{true}}{E_\text{true}} \right) dE_\text{est} \quad (9)$$

$$V(E_\text{true}) = \int R(E_\text{est}, E_\text{true}) \left(\frac{E_\text{est} - \overline{E_\text{est}}}{\overline{E_\text{est}}} \right)^2 dE_\text{est}$$
$$(10)$$

where $\overline{E_\text{est}} = \int R(E_\text{est}, E_\text{true})E_\text{est}dE_\text{est}$ is the mean estimated neutrino energy when the true neutrino energy is E_true.

A. Estimator Comparisons

Fig. 4 shows the fractional bias and variance obtained using GENIE. Among the estimators, the W^2 method exhibits the smallest overall bias. This behaviour can be understood by noting that the other estimators yield
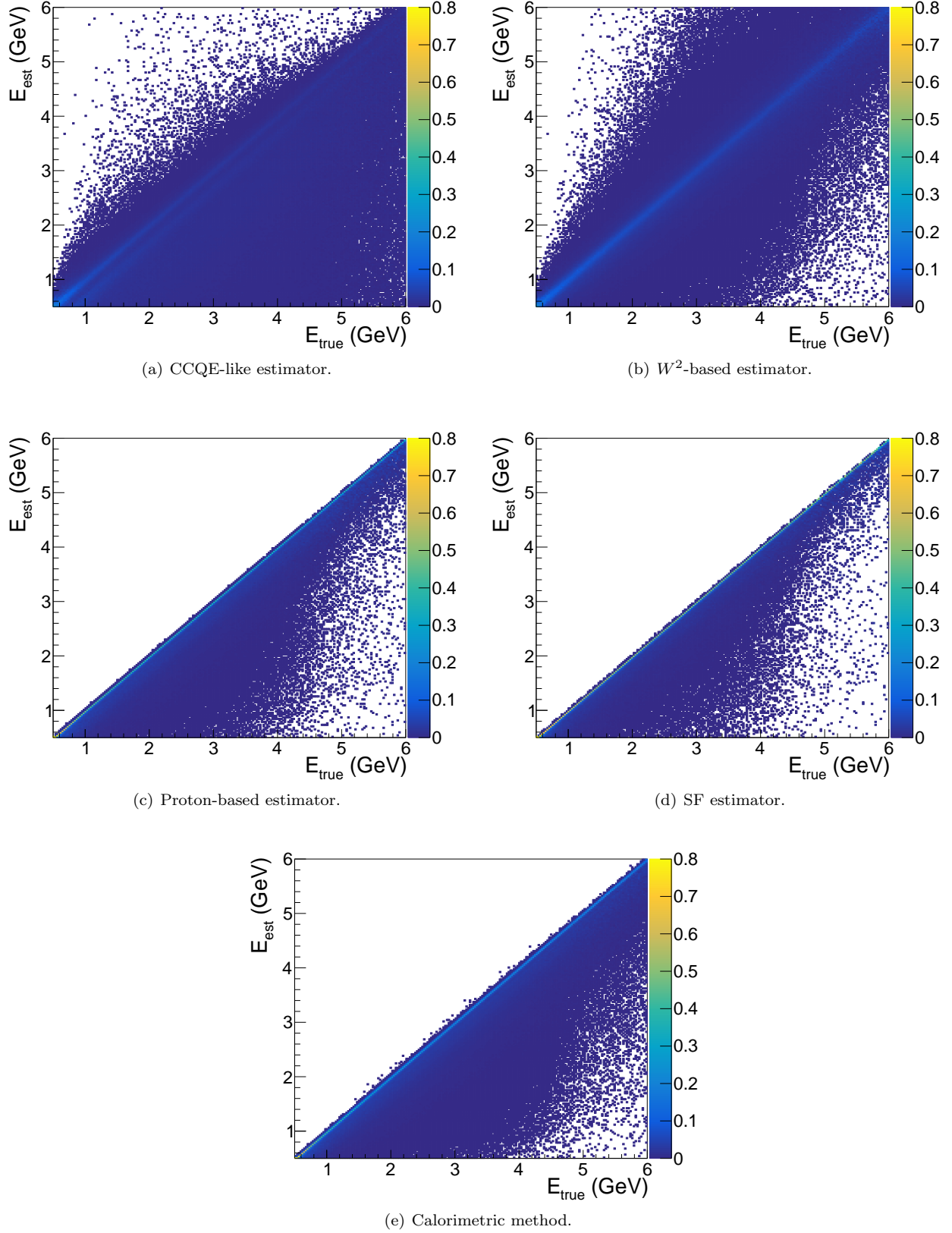
(a) CCQE-like estimator.

(b) W^2-based estimator.

(c) Proton-based estimator.

(d) SF estimator.

(e) Calorimetric method.

FIG. 2. Confusion matrices describing the smearing from true neutrino energy to estimated neutrino energy using each energy estimation.
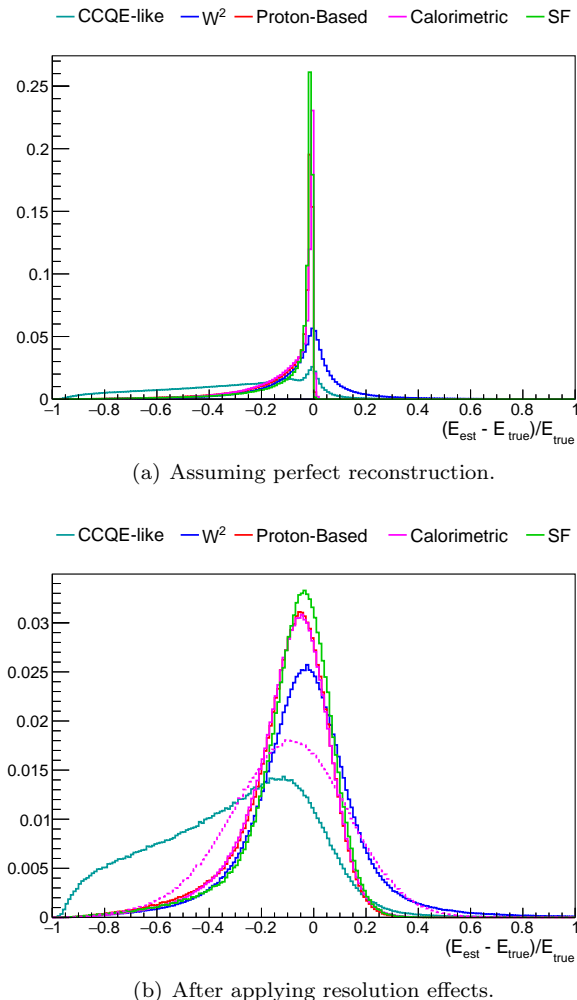
(a) Assuming perfect reconstruction.

(b) After applying resolution effects.

FIG. 3. The distribution of fractional error in neutrino energy using the different estimation methods, calculated using events simulated with the GENIE neutrino event generator. All distributions are normalized to 1. The pink dashed line is the calculation assuming overall 20% smearing on the energy calculated with the calorimetric method.

markedly asymmetric fractional error distributions, as illustrated in Fig. 3. Fig. 4(b) shows the fractional variance in the energy estimators, after including the effects of detector resolution. In the case of the calorimetric method, we show the variance when applying both the individual particle resolutions from Table II, and the overall 20% smearing (dashed line). This calculation indicates the SF method offers the best variance across most of the energy spectrum. If individual particle resolutions are applied, the calorimetric method performs the best among the more inclusive methods, though its performance suffers considerably if the more conservative 20% overall smearing is applied. This suggests experiments should consider whether to use this method if their calorimetric reconstruction performs well enough. After applying resolution effects, the performance of the SF method, proton

based methods offer similar performance, followed by the W^2 method.

Fig. 4(c) gives the increase in fractional variance for each estimator from applying the resolution effects. This indicates the the SF and proton-based methods are the least susceptible to these effects. The calorimetric method performs similarly, though this again only applies if the most optimistic model of calorimetric reconstruction in the detector is assumed. The W^2 and CCQE-like estimators are both more susceptible to resolution effects at low energies. In the case of the W^2 estimator this is because at low energies the hadronic system is often only a single proton and thus the energy estimation is purely driven by the kinematics, whereas the other methods will experience cancellations between the smearing effects to the lepton and hadronic kinematics. In the case of the CCQE-like method the resolution at higher energies is more dominated by the unrealistic assumptions this method makes about the neutrino interaction as opposed to the momentum resolution, and thus the momentum smearing is less impactful.

B. Generator Comparisons

Since realistic physics analyses typically employ multiple event generators to evaluate systematic uncertainties, we assess the robustness of each energy estimator with respect to the underlying nuclear model by varying the neutrino event generator and comparing the resulting bias and variance in the reconstructed neutrino energy. Fig. 5 shows the bias as a function of true neutrino energy for each generator. The results for the variance are provided in the Supplementary Material [19].

The benefit of the exclusive selection employed by the SF method emerges here, as the spread between the biases predicted by each generator for this estimator is noticeably smaller than that of the other estimators. It is also interesting to note that the proton-based method does not perform substantially better than the inclusive methods in this test. Of the three inclusive methods, the W^2 and calorimetric methods offer very similar performance, while the CCQE-like shows a substantial divergence between GiBUU and the other generators above 2 GeV. The predictions from GiBUU disagree with the expectation from the other three generators for all estimators at most energies, expected given GiBUU's different approach to nuclear transport modeling.

C. Focus on FSI

Final state interactions are notoriously challenging to model in neutrino interactions and can lead to substantial uncertainties in cross sections, especially for exclusive processes. We study their impact on energy estimation by comparing the bias and variance of the different energy estimation methods, calculated before and after FSI
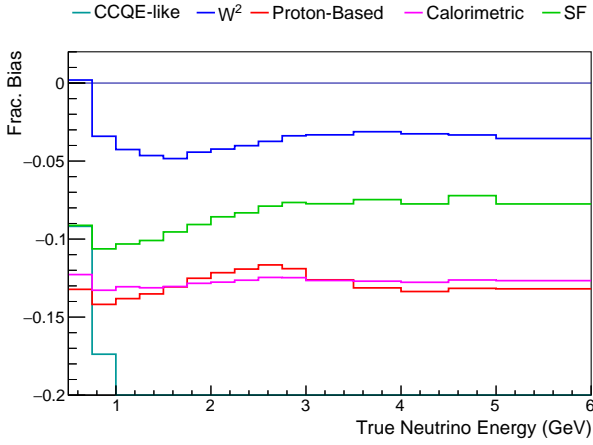
(a) Fractional bias.
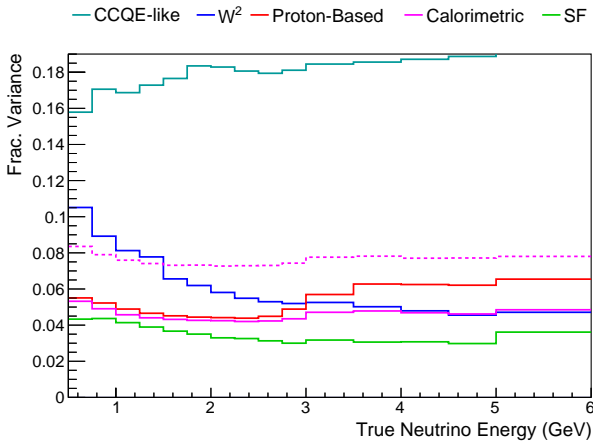
(b) Fractional variance, including resolution effects.
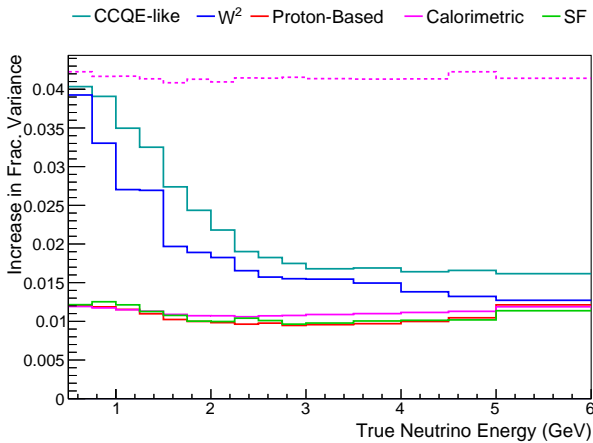
(c) Increase in fractional variance from application of resolution effects.

FIG. 4. Fractional bias and variance as a function of true neutrino energy. The dashed lines in panels (b) and (c) indicate the performance of the calorimetric method when applying the full 20% smearing to the energy estimation.

has taken place. Fig. 6 shows the bias for each estimator, calculated using both the GENIE and NuWro MC simulations. GENIE and NuWro were chosen because they provide the capability to toggle FSI on and off, enabling a controlled comparison of their effects.

The CCQE-like method is insensitive to FSI by construction, as it does not rely on information from the hadronic system. However, this conclusion carries the caveat that the factorized treatment separating FSI from the primary interaction is only an approximation of the true nuclear response.

FSI impact both the magnitude and shape of the bias for the W^2 and calorimetric methods, albeit in different ways. If GENIE is used, FSI has a minimal effect on the W^2 estimator for neutrino energies above approximately 2 GeV, and the non-FSI bias curve follows a very similar shape to the FSI one for both generators. The proton-based estimator is the most strongly affected estimator, a trend which can be seen more clearly in Figs. 6(c) and 6(d), which show the change in bias when FSI is switched on. The reliance on proton kinematics in this estimator means the visible hadronic energy in the final state is very susceptible to proton-nucleon rescattering inside the nucleus. The change in bias separates the estimators that utilise directional information from those that do not: these shifts are of a very similar shape (and magnitude when calculated with NuWro) for the W^2 and SF estimators, and likewise for the proton-based and calorimetric estimators. This calculation also exposes a noteworthy difference between the FSI modeling in NuWro and GENIE in that the change in energy bias far larger in NuWro than GENIE for most of the estimation methods.

We further check the susceptibility of each energy estimation method to FSI by calculating the fractional change in estimated neutrino energy before and after simulating FSI, and comparing the distribution of these values for each energy estimator. These distributions are shown in Fig. 7. For both generators, the SF method produces the most pronounced peak at zero, as expected, since it is explicitly designed to use transverse kinematic information to mitigate the effects of FSI. However, a shoulder and downward tail are observed when FSI are simulated with NuWro. These features are due from non-CCQE events that populate the 1p0π topology through the reabsorption of additional particles during FSI. The proton-based and calorimetric methods are the most affected by FSI, likely due to hadron absorption in the nucleus, to which estimators incorporating directional information—such as the W^2 method—are less sensitive.

(a) CCQE-like.

(b) W^2 method.

(c) Proton based.

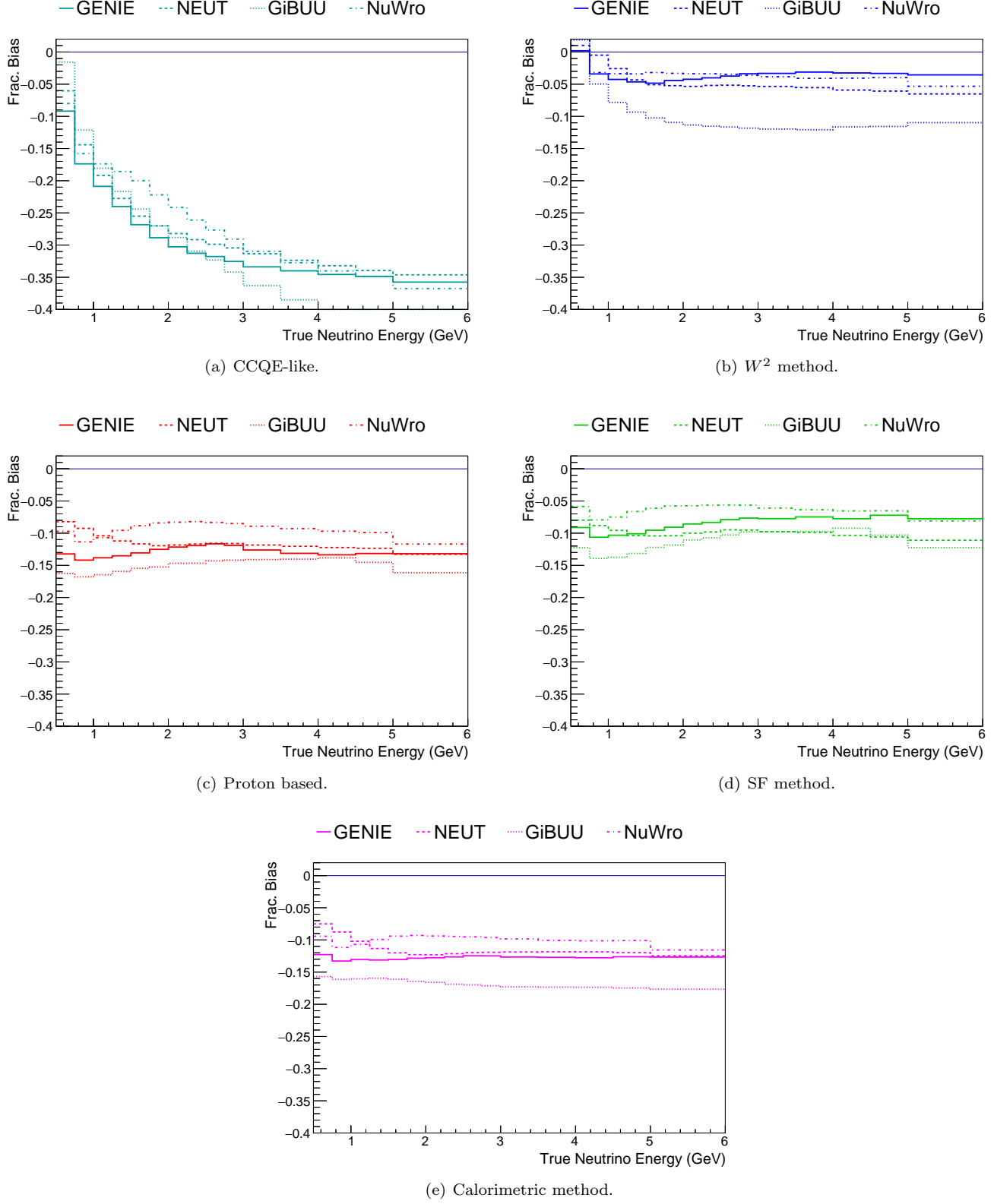(d) SF method.

(e) Calorimetric method.

FIG. 5. Comparison of the biases in neutrino energy when calculated using different event generators, for each method of neutrino energy estimation.
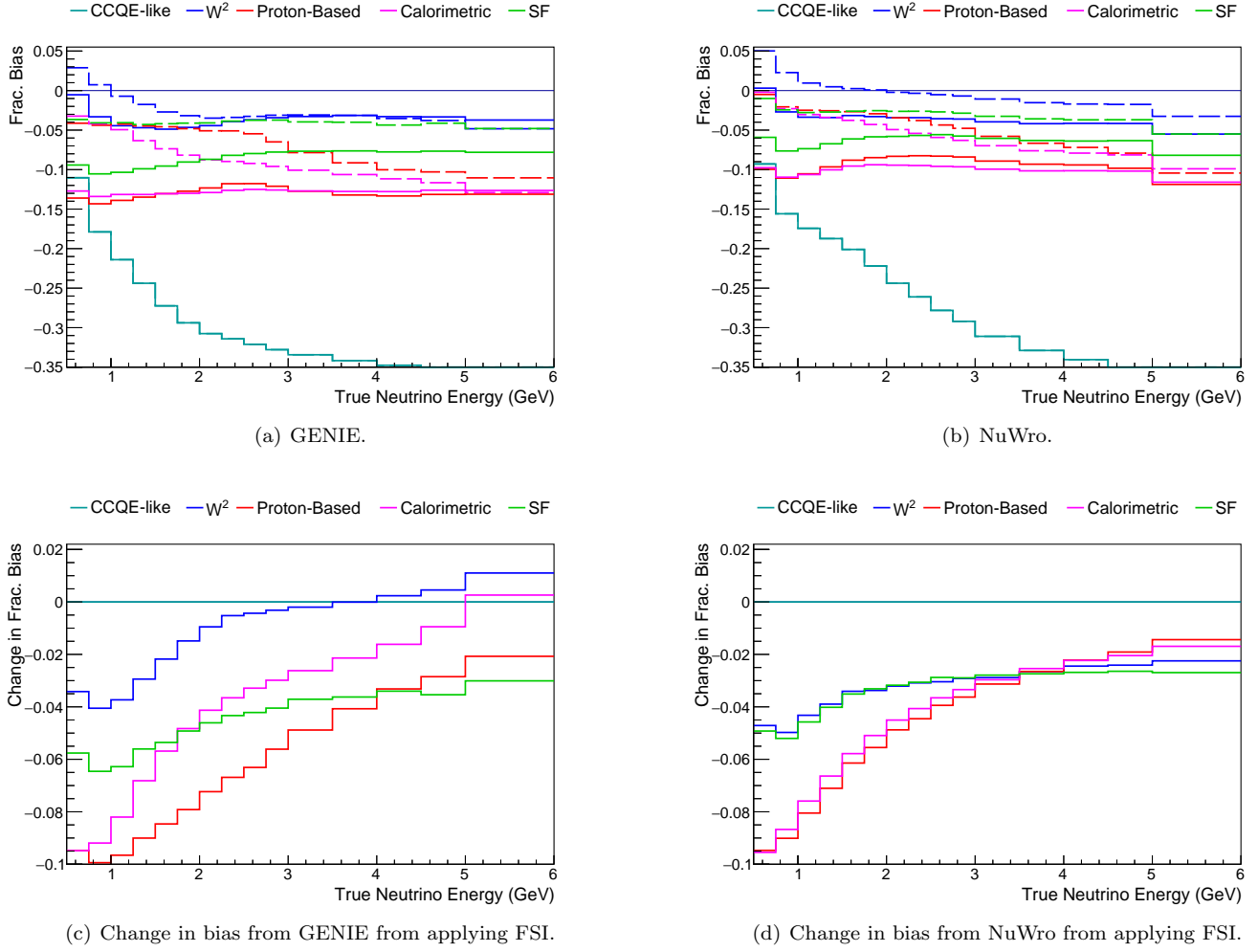
(a) GENIE.

(b) NuWro.

(c) Change in bias from GENIE from applying FSI.

(d) Change in bias from NuWro from applying FSI.

FIG. 6. Fractional bias as a function of true neutrino energy, calculated before and after simulating final state interactions. Dashed lines indicate the calculation without simulating FSI. Panels (b) and (c) show the change in the bias from switching on FSI.
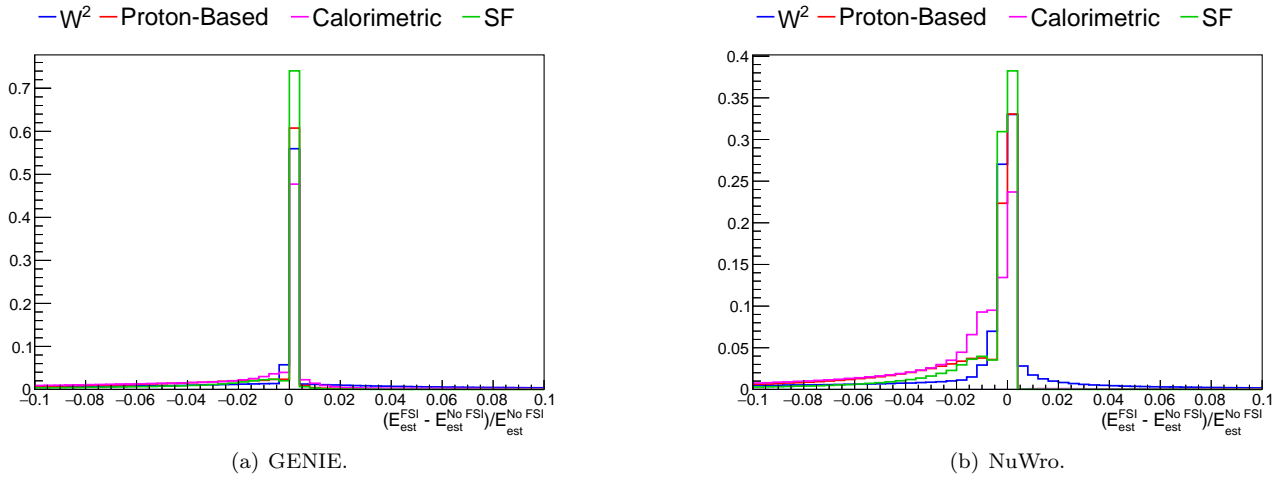

(a) GENIE.

(b) NuWro.

FIG. 7. Fractional change in the estimated neutrino energy due to FSI for each estimation method. The CCQE-like method is not displayed.

VI. SECONDARY VARIABLE DEPENDENCES

In the previous section, the bias and variance of the different energy estimators was calculated as a function of true neutrino energy. It is also important to understand if any bias and resolution effects have significant dependency on the shape of the neutrino-nucleus cross section in variables that are difficult to measure or poorly modeled. For this study, we consider the visible hadronic invariant mass, missing hadronic energy, and the lepton scattering angle – deemed as "secondary variables". We will return to the role of secondary variables in Section VII, where we evaluate their impact on the oscillation parameters.

The fractional bias and variance in neutrino energy as a function of some variable of interest x are defined as:

$$B(x) = \frac{1}{\mathcal{N}(x)} \iint \left(\frac{E_{\text{est}} - E_{\text{true}}}{E_{\text{true}}} \right) N(E_{\text{est}}, E_{\text{true}}, x) \\ dE_{\text{true}} \, dE_{\text{est}}, \tag{11}$$

$$V(x) = \frac{1}{\mathcal{N}(x)} \iint \left(\frac{E_{\text{est}} - \overline{E_{\text{est}}}(E_{\text{true}}; x)}{\overline{E_{\text{est}}}(E_{\text{true}}; x)} \right)^2 \\ N(E_{\text{est}}, E_{\text{true}}, x) dE_{\text{true}} \, dE_{\text{est}}, \tag{12}$$

where $N(E_{\text{est}}, E_{\text{true}}, x)$ is the number of events with the variable of interest at x, true neutrino energy E_{true}, and reconstructed energy E_{est}, and $\mathcal{N}(x) = \iint N(E_{\text{est}}, E_{\text{true}}, x) dE_{\text{true}} dE_{\text{est}}$ is a normalization factor. $\overline{E_{\text{est}}}(E_{\text{true}}; x)$ is the mean estimated energy of events with true energy E_{true} and variable of interest equal to x.

In this section, we use the GENIE generator as our baseline model. For completeness, we repeat the calculations with all other generators, yielding conclusions consistent with GENIE; details are provided in the Supplementary Material [19]. We find that the estimator least sensitive to the choice of generator is the CCQE-like method; however, though this apparent advantage is offset by its consistently large bias and variance across all variables examined.

A. Visible Hadronic Invariant Mass

Fig. 8 shows the bias as a function of the visible hadronic invariant mass [1]. The first notable feature is the periodic behaviour of the bias observed across all methods, most prominently in the CCQE-like estimator and, to a lesser extent, in the proton-based method. For the CCQE-like, the bias raises and falls as the true hadronic invariant mass approaches values corresponding to integer multiples of the proton mass. This pattern can be

———————

[1] We do not draw the SF method in this comparison as this is only valid when $W_{\text{vis}} = M_p$

interpreted as a larger fraction of the energy being transferred to pions when W_{vis} lies between the peaks in the W spectrum associated with specific proton multiplicities, resulting in greater bias for estimators that neglect pion information. The CCQE-like estimator exhibits a sharp increase in variance once $W > 2M_p$, marking the boundary beyond which the charged-current quasi-elastic (CCQE) hypothesis underlying this method is no longer valid. All other estimators offer similar performance, with the proton based method fluctuating depending on whether the final state invariant mass is close to an integer number of protons or not. The same periodic behavior in the variance with a period roughly equal to M_p is also present, although with a smaller effect.

B. Missing Hadronic Energy

We define the missing hadronic energy as the sum of the kinetic energies of all neutrons, the kinetic energies of protons and total energies of pions below the detection threshold. Fig. 9 shows the distributions of bias and variance in neutrino energy as a function of missing hadronic energy. The distribution of bias produced by the W^2 method and CCQE-like methods are flatter than the other estimators, implying greater stability with respect to the variation of missing energy, though this benefit is partially offset by the greater variance shown in Fig. 9(b). It is interesting to note the SF method is still susceptible to the presence of missing energy despite being constructed to infer the its impact through missing transverse momentum. Comparison of this figures with the corresponding bias distributions from the visible invariant mass and lepton angle shows that the missing hadronic energy has the potential to create the largest bias in neutrino energy.

C. Angular Dependency

One of the features that distinguishes the CCQE-like, W^2, and SF estimators from the other methods is that they include angular information in their calculation, in contrast with the proton-based and calorimetric methods which purely utilize the kinetic (or total) energies of final state particles, irrespective of their directions. Fig. 10 shows the fractional bias and variance as a function of lepton scattering angle θ. The bias calculation reveals the improvement made to the purely muon kinematics method by accounting for the invariant mass of the full final state, as the muon kinematics increasingly underestimates the neutrino energy as the scattering angle increases. At very large angles the interaction will be highly inelastic making the quasielastic approximation inaccurate, leading to large bias. The W^2 method overall performs well in this test as the bias is very close to flat as a function of lepton angle, while all other estimators trend downward.

(a) Fractional bias.

(b) Fractional variance.
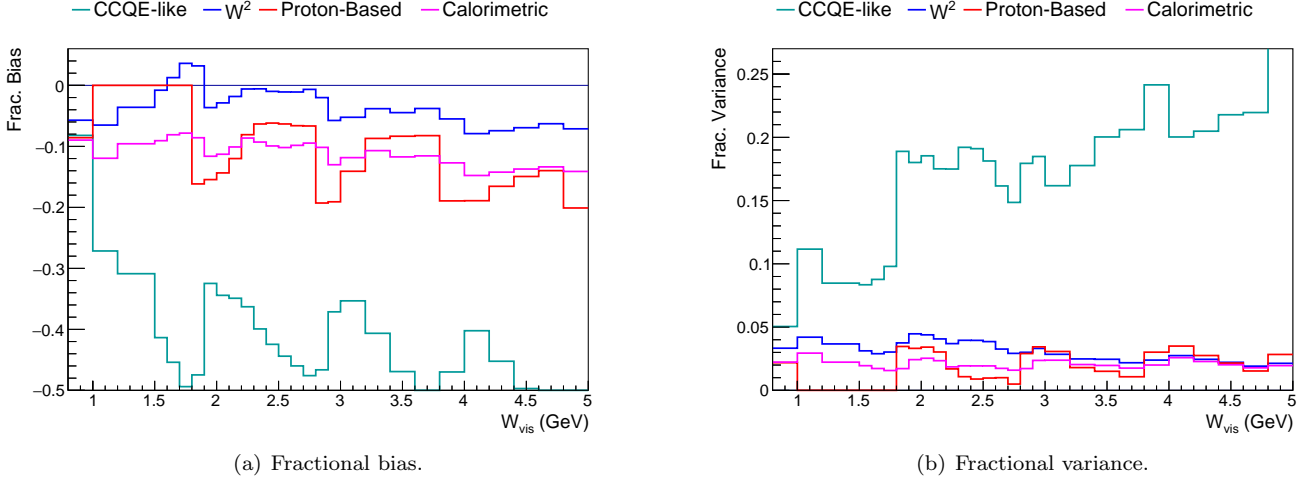
FIG. 8. Fractional bias and variance as a function of visible hadronic invariant mass.

(a) Fractional bias.

(b) Fractional variance.
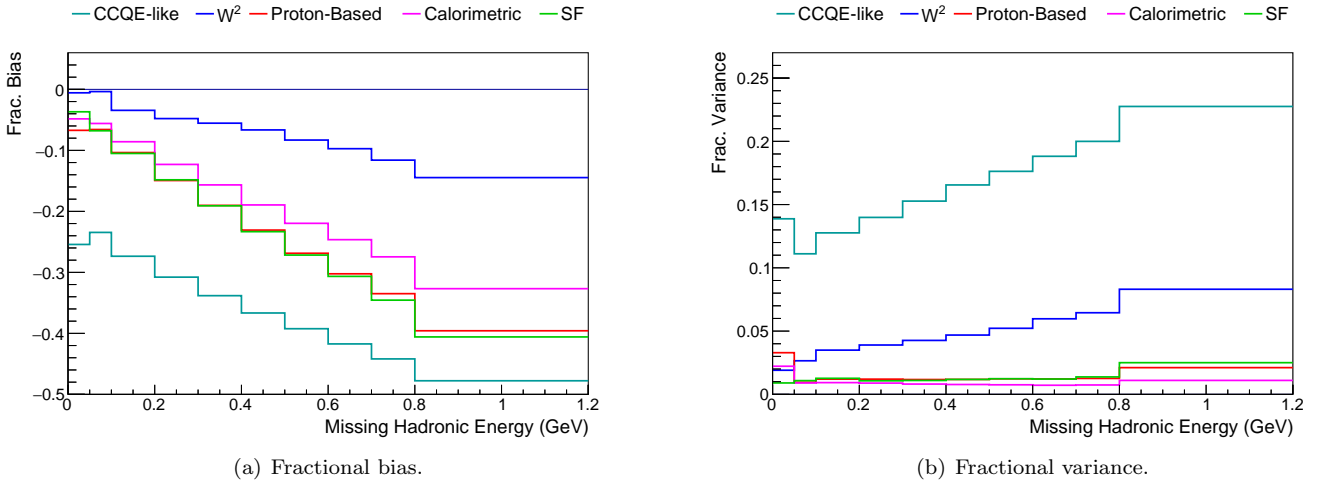
FIG. 9. Fractional bias and variance as a function of missing hadronic energy.
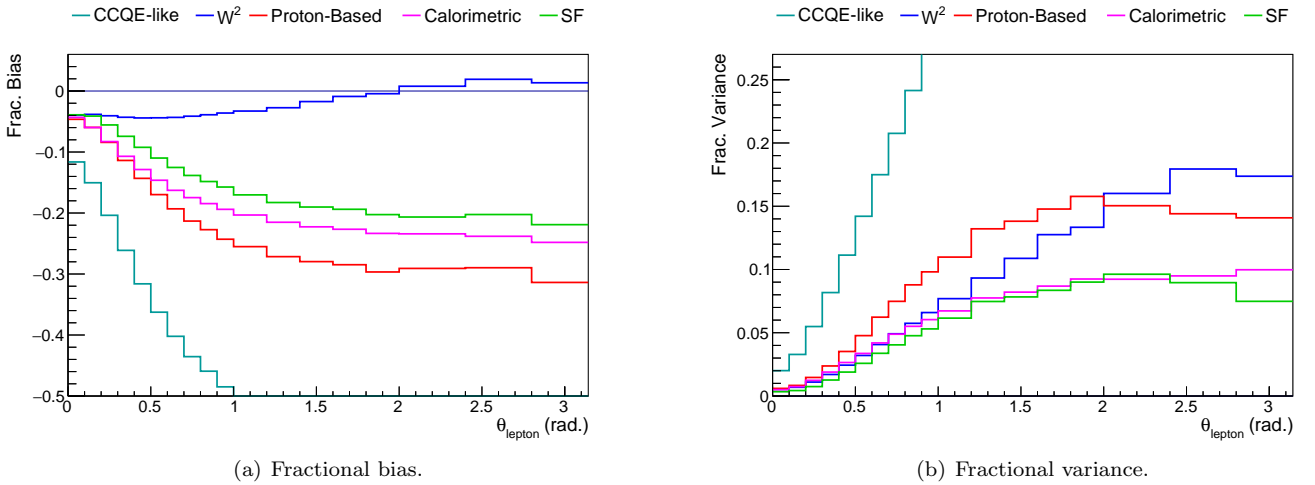

(a) Fractional bias.

(b) Fractional variance.

FIG. 10. Fractional bias and variance as a function of the lepton scattering angle.

VII. IMPACT OF ESTIMATOR CHOICE ON OSCILLATION PARAMETERS

In this section, we examine how the choice of energy estimator influences oscillation measurements, with the aim of identifying which estimator provides the most robust inference of oscillation parameters. Here, robustness refers to reduced susceptibility to biases arising from the choice of event generator in general and from final-state interactions (FSI) in particular. Since the connection between reconstructed neutrino energy and oscillation parameter inference is non-trivial, the CP-violating phase δ_{CP} is probed using a toy ν_e-appearance analysis at the far detector, while the mass-splitting Δm_{32}^2 is constrained through "shape-only" fits of ν_μ disappearance spectra. We make no assumption regarding a near detector constraint.

A. Estimator Comparison in Parameter Exclusion

We compare the performance of different energy estimators in excluding benchmark oscillation hypotheses when specific alternate parameters are assumed. We consider two tests: excluding the global central value of $\Delta m_{23}^2 = 2.451 \times 10^{-3}$ eV^2 [20] using ν_μ disappearance, and excluding $\delta_{CP} = 0$ with ν_e appearance, both assuming DUNE's far detector flux and baseline.

For each estimator/generator combination, we compute the estimated energy spectra from ν_μ assuming the central value and the central value $\pm 3\sigma$, where $\sigma = 0.026 \times 10^{-3}$ eV^2 [20]. All distributions are normalized to the same arbitrary detector exposure. We then compute the following metric to quantify the strength of the exclusion of the central value:

$$\sqrt{X} = \sqrt{\sum_i \left(\frac{N_i' - N_i}{\sqrt{N_i'}} \right)^2}, \qquad (13)$$

where N_i is the predicted rate in the ith estimated energy bin assuming the central value, and N_i' is the rate assuming the central value $\pm 3\sigma$. Similarly, in the ν_e appearance case, we treat $\delta_{CP} = 0$ as the central value and compute N_i' using $\delta_{CP} = \pm\frac{\pi}{2}$.

Figure 11 compares the performance of the different estimators relative to a benchmark case: GENIE using the W^2 estimator. The performance metric is expressed as the ratio of the $\sqrt{X}$ values obtained for each estimator-generator combination to the benchmark case, which allows for a formulation independent of the overall exposure.

For a fixed estimator, there is a substantial spread in performance across generators. By exhibiting a smaller generator-to-generator spread, the SF method appears marginally more robust against model dependence – a result consistent with the smaller spread in bias observed in Fig 5. However, the SF method consistently provides the weakest separation power. For a fixed generator the

relative ordering of estimators is fairly consistent, with the calorimetric and W^2 estimators providing the best separation power.

In ν_μ disappearance, exclusive methods such as SF or proton-based offer competitive sensitivity, but in ν_e appearance the loss of statistics outweighs gains in robustness. This highlights the importance of inclusive estimators for CP-violation searches.

B. Final State Interactions

We define the estimated energy spectrum for a given estimator as

$$N(E_{\text{est}}; \alpha) = \int R(E_{\text{est}}, E_{\text{true}}) \, P(E_{\text{true}}; \alpha) \, \Phi(E_{\text{true}}) \, dE_{\text{true}}, \qquad (14)$$

where $R(E_{\text{est}}, E_{\text{true}})$ is the response matrix, $P(E_{\text{true}}; \alpha)$ the oscillation probability, and $\Phi(E_{\text{true}})$ the incident flux. The parameter set α denotes the oscillation parameter of interest, i.e. δ_{CP} in the ν_e appearance channel and Δm_{32}^2 in the ν_μ disappearance channel. When analyzing the FSI impact, we will only consider Δm_{32}^2 and ν_μ disappearance; we will explore the impact of mismodelling secondary variables on δ_{CP} measurements in Section VIII. We inject different assumptions (e.g. FSI on or off) in the estimated energy spectra by replacing the response matrix in equation 14.

To study the effect of FSI, we build two estimated spectra, one using the response matrix with the full simulation and one made without simulating FSI. We denote the two estimated energy spectra as $N(\alpha)$ and $N'(\alpha')$ respectively, in which different sets of oscillation parameters, α and α' have been used in equation 14. We restrict the fit range between true neutrino energies of 0.8 GeV and 5.0 GeV, fitting only the two largest oscillation minima/maxima. We then perform a closure test in which the spectrum constructed without simulating FSI in the response matrix is fitted to spectrum made with the full simulation by varying α' to minimize:

$$X(\alpha') = \sum_i \left(\frac{N_i'(\alpha') - N_i(\alpha)}{\sqrt{N_i(\alpha)}} \right)^2, \qquad (15)$$

where again i indexes the bins in the estimated neutrino energy spectrum. The difference between the best fit of α' and the value of α used to construct the original spectrum with the full simulation then quantifies the impact of FSI in an oscillation context.

Fig. 12 shows the ratio between the extracted value of Δm_{23}^2 obtained from fitting the non-FSI spectrum with equation 15 and the value of Δm_{23}^2 used to generate the full spectrum with FSI. Consistently with Section V C, the impact of FSI on the oscillation parameters is smallest when using the W^2 and SF estimators, whereas the use of calorimetric and proton-based methods display sizable biases. The behavior is consistent across GENIE and NuWro.
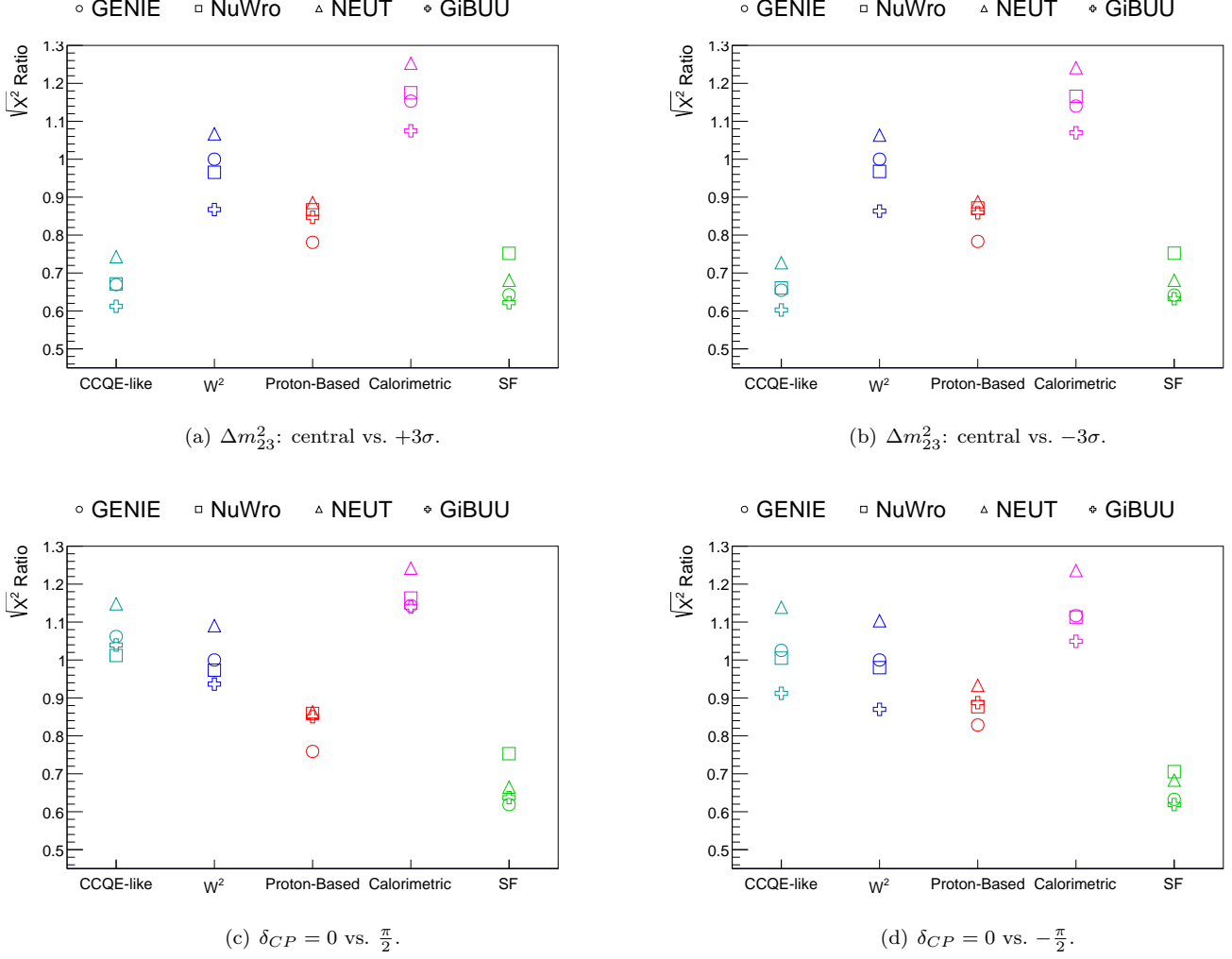
(a) Δm_{23}^2: central vs. $+3\sigma$.

(b) Δm_{23}^2: central vs. -3σ.

(c) $\delta_{CP} = 0$ vs. $\frac{\pi}{2}$.

(d) $\delta_{CP} = 0$ vs. $-\frac{\pi}{2}$.

FIG. 11. Relative exclusion power of different estimators, expressed as the ratio of $\sqrt{\chi^2}$ to the GENIE W^2 baseline.
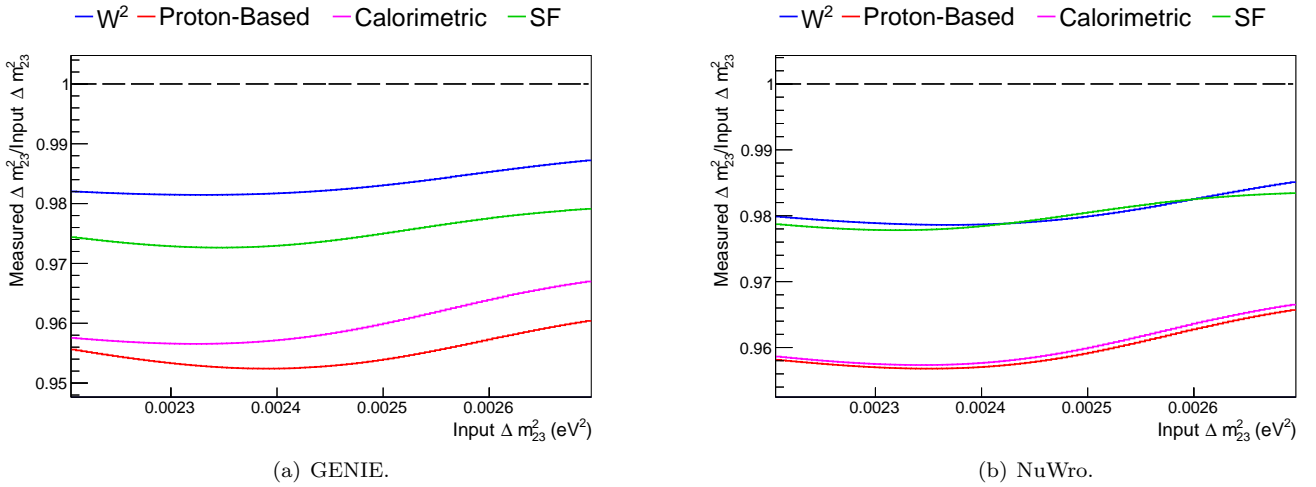

(a) GENIE.

(b) NuWro.

FIG. 12. Bias in extracted Δm_{32}^2 when fitting spectra generated with and without FSI.

VIII.   IMPACT OF SECONDARY VARIABLES DEPENDENCY

We perform a variation of the closure test described in Section VII B to explore the impact of secondary variables (defined in Section VI) on the oscillation parameter extraction. Here, instead of switching off final state interactions to yield a modified response matrix, we construct a series of alternative response matrices by changing the event selection on one of the three secondary variables. We then investigate how the mismodelling of these variables affects the inferred oscillation parameters by fitting the alternative spectrum obtained from the modified response matrix in Eq. 14, and re-minimizing the function in Eq. 15 to extract the corresponding parameter α'.

We perform this test considering both ν_μ disappearance and Δm_{23}^2, and ν_e appearance and δ_{CP}. Contrary to our FSI study, we only consider the global central value of Δm_{23}^2, and $\delta_{CP} = \{0, \frac{\pi}{2}, -\frac{\pi}{2}\}$ to study how varying the selection on the hidden variable influences inference.

We find it is also informative to calculate the shift in the overall bias in neutrino energy across the entire MC simulation sample, $B' - B$, as a function of the selection on the secondary variable. These calculations are shown in Figures 17, 15, and 13 and often mimic the bias in the extracted oscillation parameters resulting from the cut on the hidden variable (up to the sign of the bias, as this depends on the oscillation parameter in question).

A.   Hadronic Invariant Mass

The oscillation closure tests are produced from cutting on the visible hadronic invariant mass are shown in Fig. 14. We build the alternative response matrix by placing an upper limit on W_{vis}, starting at the single proton mass and gradually allowing more complex final states. We see periodic "bends" in the bias in extracted oscillation parameters, similar to the features in the bias in neutrino energy previously seen in Fig. 8, particularly when W approaches integer multiples of the nucleon mass. These underscore the importance of accurate multi-nucleon and resonance modeling in neutrino generators. Comparison of the biases across different estimators indicates the W^2 method closes for largest portion of the parameter space, followed closely by the calorimetric method. We do not draw the CCQE-like result for portions of the parameter space in the δ_{CP} fits as the bias in this case cannot be offset by modifying the value of δ_{CP} alone.

B.   Missing Hadronic Energy

We explore the impact of missing hadronic energy through constructing the alternative response matrix with an upper limit on this quantity, starting with only events in which all hadronic energy is visible. The results of this closure test are presented in Fig. 16. As expected, the SF method demonstrates the greatest resilience, as this method is able to infer missing momentum from invisible particles, followed by the W-based and proton-based estimators. The calorimetric and CCQE-like methods are more sensitive to unobserved hadronic components.

C.   Angular Dependence

We also construct the alternative response matrix by cutting on the lepton scattering angle, starting with only including forward going leptons before loosening the cut to include larger angles, corresponding to more inelastic interactions. Fits of the oscillated spectra are shown in Fig. 18, revealing that the W-based estimator is comparatively stable, while the purely CCQE-like approach is highly susceptible to angle mismodelling. The SF method offers the second best performance, likely because this method is applied to selected events that still resemble quasielastic interactions even at large scattering angles.
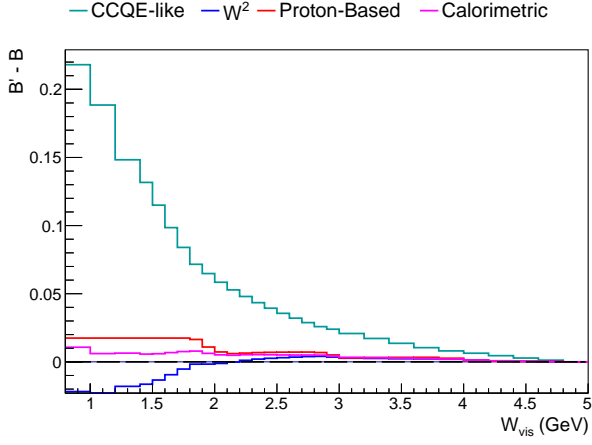
FIG. 13. Dependence of energy bias on visible hadronic invariant mass. Sharp structures occur near integer multiples of the nucleon mass, reflecting sensitivity to resonance and multi-nucleon production.
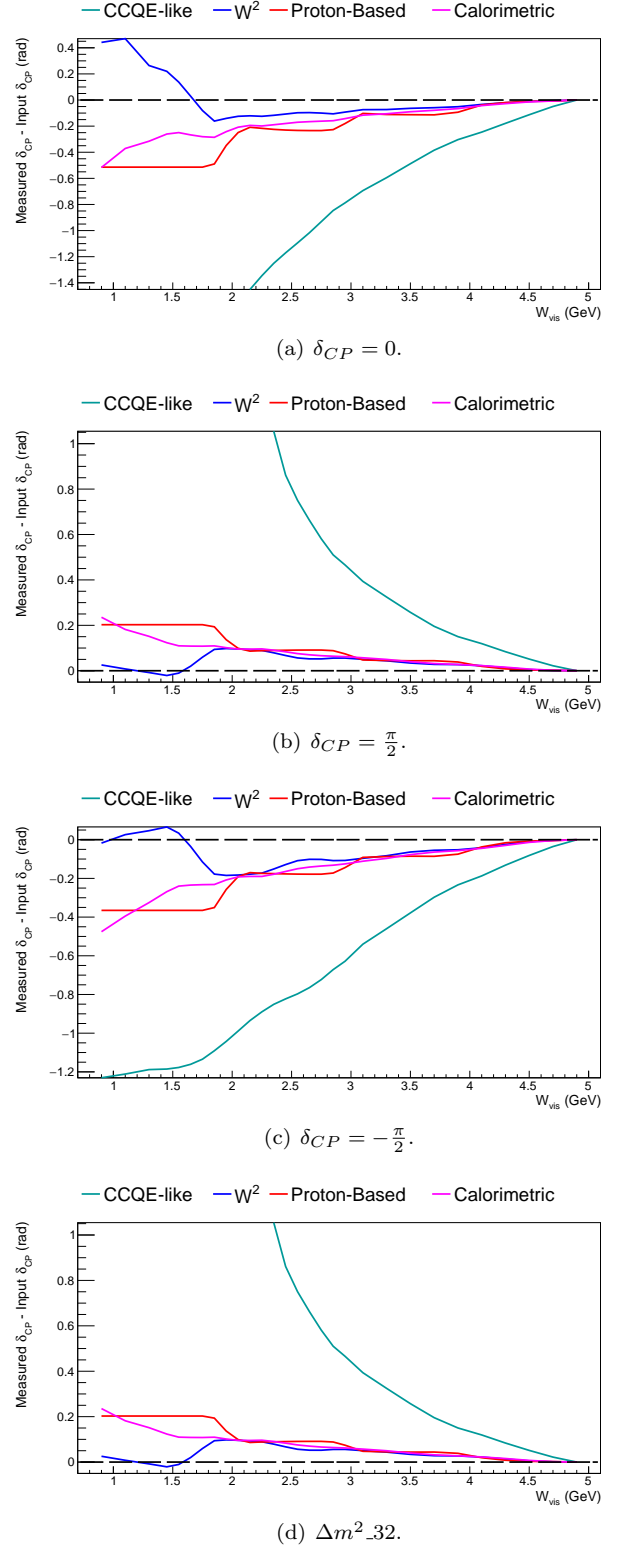

(a) $\delta_{CP} = 0$.

(b) $\delta_{CP} = \frac{\pi}{2}$.

(c) $\delta_{CP} = -\frac{\pi}{2}$.

(d) Δm^2_32.

FIG. 14. Oscillation fits when events are selected by visible hadronic invariant mass. Periodic structures in the extracted δ_{CP} and Δm^2_{32} reflect the resonance-like features in Fig. 14.
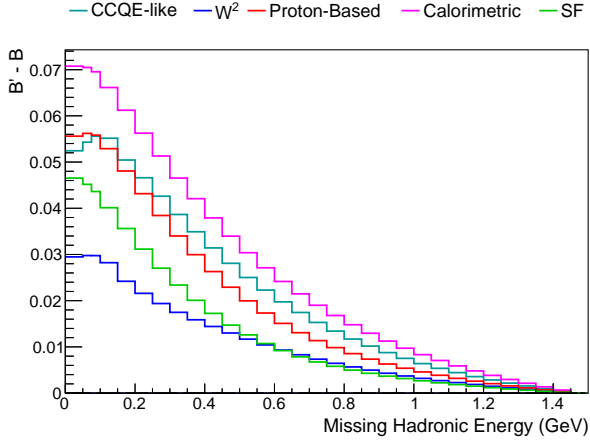
FIG. 15. Change in reconstructed energy bias as a function of missing hadronic energy. Methods that incorporate transverse kinematic balance (SF, W-based) remain stable, whereas calorimetric and muon-kinematic methods degrade more strongly.
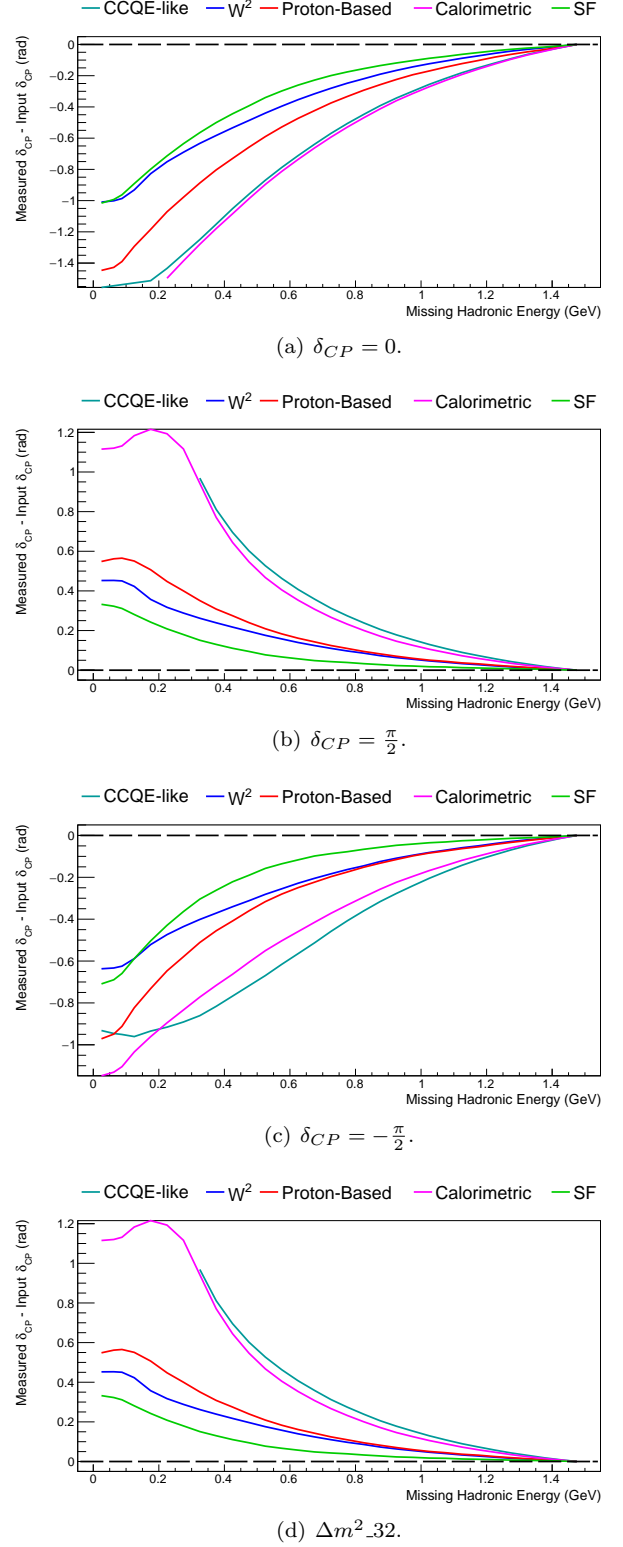

(a) $\delta_{CP} = 0$.

(b) $\delta_{CP} = \frac{\pi}{2}$.

(c) $\delta_{CP} = -\frac{\pi}{2}$.

(d) Δm^2_32.

FIG. 16. Oscillation fits under restrictions on missing hadronic energy. The SF method yields the most consistent δ_{CP} and Δm^2_{32} extraction, though with reduced statistics.
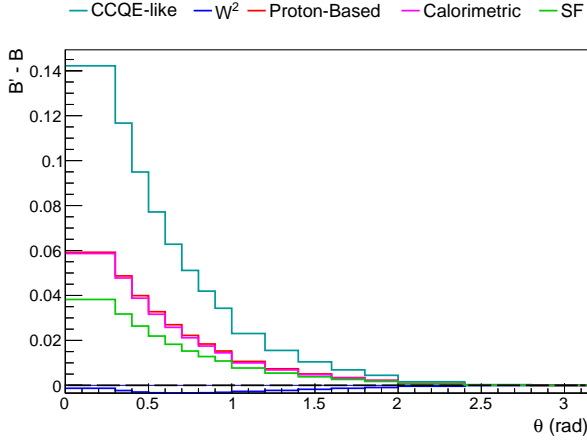
FIG. 17. Change in average bias as a function of a cut on lepton scattering angle, comparing all estimators. Forward-going selections reduce the impact of angular mismodelling, with the W-based method showing the most stable behavior.
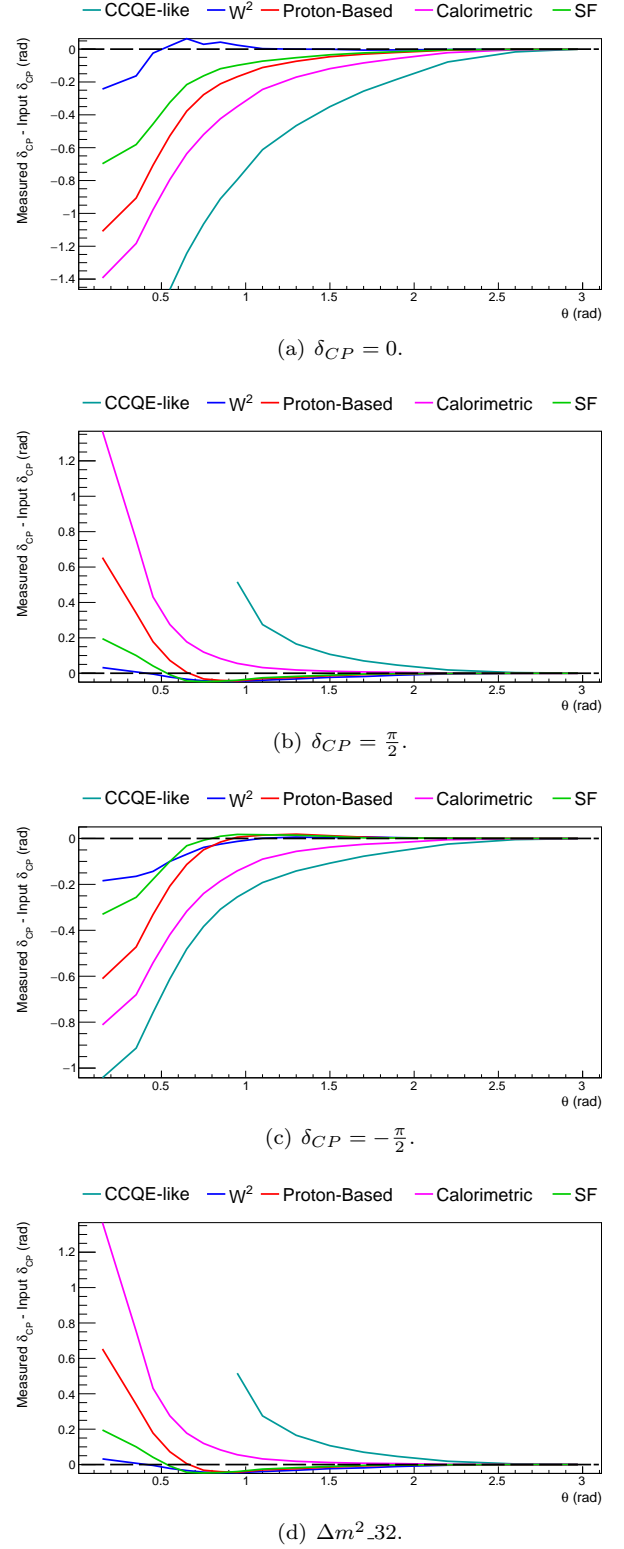

(a) $\delta_{CP} = 0$.

(b) $\delta_{CP} = \frac{\pi}{2}$.

(c) $\delta_{CP} = -\frac{\pi}{2}$.

(d) Δm^2_32.

FIG. 18. Extracted oscillation parameters when restricting events by lepton scattering angle. The W-based estimator converges rapidly to the correct δ_{CP} and Δm^2_{32} values, while the muon-only approach shows strong dependence on θ.

IX. SUMMARY

In this work, we investigate a new method to estimate neutrino energy in broadband beams based on the measurement of the final-state hadronic invariant mass, W. This method is compared against several other commonly used estimators: the CCQE kinematics formula, summation of the energies of final state protons, a calorimetry based approach, and the Sobczyk-Furmanski method.

The W^2 method consistently exhibits the smallest overall bias as functions of the true energy, with a variance comparable to other inclusive estimators, particularly once resolution effects are considered. Additionally, the W^2 method shows the weakest dependence on FSI effects, most notably when using the GENIE neutrino event generator. When probing the stability of each estimator against the visible hadronic invariant mass, missing hadronic energy, and lepton scattering angle, we find that the W^2 method often shows the least variation in bias with respect to these variables, especially in the case of the lepton's scattering angle.

These findings are mirrored in an oscillation analysis context. The most powerful methods in the exclusion tests are the calorimetric, W^2, and CCQE-like estimators. While the Sobczyk–Furmanski method achieves the lowest variance, its sensitivity in the toy oscillation analyses is reduced due to the substantial loss of statistics. In the closure tests, the W^2 method emerges as the most stable among the inclusive estimators, particularly with respect to FSI effects, often exhibiting the smallest bias in the extracted oscillation parameters across the widest regions of parameter space.

In this work, we examine each method individually, highlighting the contexts and underlying motivations for which each estimator performs best. This thorough examination provides a detailed guidance for future experiments on how to combine estimators to enhance overall performance.

ACKNOWLEDGMENTS

[1] K. Abe *et al.* (T2K), Constraint on the matter–antimatter symmetry-violating phase in neutrino oscillations, Nature **580**, 339 (2020), [Erratum: Nature 583, E16 (2020)], arXiv:1910.03887 [hep-ex].

[2] P. A. Machado, O. Palamara, and D. W. Schmitz, The Short-Baseline Neutrino Program at Fermilab, Ann. Rev. Nucl. Part. Sci. **69**, 363 (2019), arXiv:1903.04608 [hep-ex].

[3] R. Acciarri *et al.* (DUNE), Long-Baseline Neutrino Facility (LBNF) and Deep Underground Neutrino Experiment (DUNE): Conceptual Design Report, Volume 2: The Physics Program for DUNE at LBNF, (2015), arXiv:1512.06148 [physics.ins-det].

[4] R. Acciarri *et al.* (DUNE), Long-Baseline Neutrino Facility (LBNF) and Deep Underground Neutrino Experiment (DUNE): Conceptual Design Report, Volume 1: The LBNF and DUNE Projects, (2016), arXiv:1601.05471 [physics.ins-det].

[5] A. P. Furmanski and J. T. Sobczyk, Neutrino energy reconstruction from one muon and one proton events, Phys. Rev. C **95**, 065501 (2017), arXiv:1609.03530 [hep-ex].

[6] J. Kopp, P. Machado, M. MacMahon, and I. Martinez-Soler, Improving neutrino energy reconstruction with machine learning, (2024), arXiv:2405.15867 [hep-ph].

[7] C. Andreopoulos *et al.*, The GENIE Neutrino Monte Carlo Generator, Nucl. Instrum. Meth. A **614**, 87 (2010), arXiv:0905.2517 [hep-ph].

[8] J. Sobczyk, A. Ankowski, K. Graczyk, C. Juszczak, K. Niewczas, R. Banerjee, H. Prasad, *et al.*, NuWro: Monte Carlo Neutrino Event Generator User's Guide, https://nuwro.github.io/user-guide/ (2024), accessed 2025.

[9] Y. Hayato, NEUT, Acta Phys. Polon. B **33**, 2469 (2002).

[10] O. Buss, T. Gaitanos, K. Gallmeister, H. van Hees, M. Kaskulov, O. Lalakulich, A. Larionov, T. Leupold, J. Weil, and U. Mosel, Transport-theoretical Description of Nuclear Reactions, Phys. Rept. **512**, 1 (2012).

[11] A. Friedland and S. W. Li, Understanding the energy resolution of liquid argon neutrino detectors, Phys. Rev. D **99**, 036009 (2019), arXiv:1811.06159 [hep-ph].

[12] P. Abratenko *et al.* (MicroBooNE), Measurement of single charged pion production in charged-current ν_μ-Ar interactions with the MicroBooNE detector, (2025), arXiv:2509.03628 [hep-ex].

[13] P. Abratenko *et al.* (MicroBooNE), Measurement of the differential cross section for neutral pion production in charged-current muon neutrino interactions on argon with the MicroBooNE detector, Phys. Rev. D **110**, 092014 (2024), arXiv:2404.09949 [hep-ex].

[14] P. Abratenko *et al.* (MicroBooNE), First study of neutrino angle reconstruction using quasielasticlike interactions in MicroBooNE, Phys. Rev. D **111**, 113007 (2025), arXiv:2504.17758 [hep-ex].

[15] P. Abratenko *et al.* (MicroBooNE), Differential Cross Section Measurement of Charged Current νe Interactions Without Pions in MicroBooNE, Phys. Rev. D **106**, L051102 (2022), arXiv:2208.02348 [hep-ex].

[16] C. Adams *et al.* (MicroBooNE), Calibration of the charge and energy loss per unit length of the MicroBooNE liquid argon time projection chamber using muons and protons, JINST **15** (03), P03022, arXiv:1907.11736 [physics.ins-det].

[17] P. Abratenko *et al.* (MicroBooNE), Search for an anomalous excess of charged-current νe interactions without pions in the final state with the MicroBooNE experiment, Phys. Rev. D **105**, 112004 (2022), arXiv:2110.14065 [hep-

ex].

[18] P. Abratenko *et al.* ((MicroBooNE Collaboration)*, MicroBooNE), Search for an Anomalous Production of Charged-Current νe Interactions without Visible Pions across Multiple Kinematic Observables in MicroBooNE, Phys. Rev. Lett. **135**, 081802 (2025), arXiv:2412.14407

[hep-ex].

[19] See Supplemental Material.

[20] S. Navas *et al.* (Particle Data Group), Review of particle physics, Phys. Rev. D **110**, 030001 (2024).